An Innovative Solar-Assisted Compressed Air Energy Storage System Integrated with a Liquefied Air Power Cycle

Shayan Sadeghi[1], Samane Ghandehariun[1], Behnaz Rezaie[2], Nader Javani[3]

[1]Sustainable Energy Research Group (SERG), School of Mechanical Engineering, Iran University of Science and Technology, Tehran, Iran
[2]Applied Energy Research Laboratory (AERL), Department of Mechanical Engineering, College of Engineering, University of Idaho, 875 Perimeter Dr., Moscow, ID 83844-0902, USA
[3]Faculty of Mechanical Engineering, Yildiz Technical University, 34349, Istanbul, Turkey

Abstract

In the present study, a novel solar-based integrated compressed air energy storage system is developed and analyzed. The integrated system includes a multi-stage air compression unit, thermal oil loop, multi-stage gas turbine unit, high-temperature molten salt-based solar power tower unit, liquefied air power cycle, thermoelectric generator, and liquefied natural gas (LNG) regasification unit. A eutectic mixture of carbonate salt is used for thermal energy storage in the solar subsystem. Energy and exergy analyses are performed to evaluate the performance of the proposed system. A parametric study is also conducted to assess the effects of important parameters on system performance. The system stores 55.3 MW power during charging mode and discharges 99.7 MW. Energy and exergy efficiencies of the integrated system are 55.3% and 46.4%, respectively. The results show that the highest contributor to the overall exergy destruction rate of the system is the combustion chamber unit.

Keywords: Compressed air energy storage; Solar energy; Liquefied air power cycle; Exergy analysis; LNG regasification; Thermal energy storage

1. Introduction

With the exhaustion of fossil fuel resources and aggravation of global energy demand, the utilization of renewable energies to achieve sustainability has become an important subject of research and development in the modern era [1]. One of the main challenges associated with renewable energies is their intermittent nature [2]. To deal with this obstacle and to manage the outgrowing problems of high energy demand, it is necessary to use energy storage systems which store energy when it is not needed and use it later when the demand is high [3].

Energy may be stored in the form of mechanical, chemical, or thermal energy [4]. Compressed air energy storage (CAES), as a mechanical energy storage method, is one of the most promising methods to resolve the intermittent issues of renewable energies [5]. This method possesses various advantages including technology maturity, availability of equipment, low investment cost, and high energy storage capacity [6,7].

CAES systems store energy through a series of air compressors to pressurize and store atmospheric air in underground reservoirs such as salt caverns or high-pressure tanks above

ground. When energy is required, the pressurized air flows through a series of expansion units in order to generate power [8]. To increase the system efficiency, it is convenient to use the heat generated in the compression process to heat up the air before entering the expanders [8]. Liu et al. [9] investigated the CAES system through an advanced exergetic analysis. Their results indicated that the round-trip and exergy efficiencies of the cycle were 47.4% and 41.2%, respectively. Advanced exergetic analysis showed that 34.6 MW of the total exergy destruction of the system is not related to the irreversibilities, and therefore, it is avoidable. More specifically, intercooler, aftercooler, and combustion chamber accounts for around 58% of the avoidable exergy destruction in the system [9]. In a comparative study, Krawczyk et al. [10] investigated two compressed air energy storage systems including a conventional diabatic CAES and a liquefied air energy storage (LAES). The round-trip efficiency of the CAES and LAES systems were reported as 39.77 and 55.2%, respectively [10]. Peng et al. [11] proposed and analyzed an adiabatic CAES system coupled with a packed bed thermal energy storage system and overall efficiency of 56.74% was reported for their design [11]. In another comparative study, Liu and Wang [12] investigated two different adiabatic CAES systems for energy storage. One of which was a conventional CAES system and the other was a modified version of CAES that used a pneumatic motor, heat accumulator, and preheater. The results indicated that the modified version had a round trip efficiency of 66.9% which is 13% higher than that of the conventional CAES system [12]. Coupling of the CAES system with the Kalina cycle was proposed by Zhao et al. [13]. Kalina cycle is used to recover the waste heat of the CAES system and a round trip efficiency of 47.64% was reported [13]. In another study, Szablowski et al. [14] investigated an adiabatic CAES system in terms of energetic and exergetic perspectives. The round-trip efficiency of their proposed cycle was 50% [14]. A transient thermodynamic model for an underwater CAES system was developed and investigated by Carriveau et al. [15]. The results indicated that the heat exchangers are the main contributors to the exergy destruction of the system with a value of 29% while considering steady-state condition. On the other hand, under transient condition, the highest exergy destruction contributors are air compressors with a value of 40% of the total exergy destruction of the system [15].

For increasing the performance of gas turbines (GT) or CAES systems, one convenient way is to use natural gas to achieve higher temperature for the inlet of the gas turbines [16]. As the outlet temperature of the gas turbine is high, they can be coupled with a bottoming cycle to increase the performance of the system [16]. A commonly used combined power cycle utilizes a steam Rankine cycle coupled with the gas turbine units for this mean [17]. Natural gas is mostly liquefied in order to be transported more efficiently in large distances. When it is needed again, it is regasified using cryogenic pumps, heat exchangers, and expanders. The cold waste heat of this process can be used as a heat sink of many power generation processes to yield additional power and increase the cycle performance [18]. Several working fluids are suitable for this purpose [19]. As an example of the compressed gas energy storage, the feasibility of compressed carbon dioxide energy storage (CCES) integrated with low-temperature thermal energy storage has been studied in the literature [20] in which the results show the feasibility of the cycle to be used in cogeneration systems. For the assessment of compressed air energy storage systems, the heat transfer mechanism and heat losses from the storage tank or cavern should be considered. An experimental and theoretical study has been conducted for a high-pressure compressed air tank storage system in which the experimental data was used to assess the wall and air temperatures in the pressurized storage tank

of 100 bar. The results showed that the tank wall should be taken into account in the thermal analysis of CAES systems [21]. In another study, a compressed air energy storage is integrated with a biomass-driven power plant with thermal energy storage subsystems. Similar to the previous reference, the effect of heat loss in the cavern and the temperature of the soil around the cavern on the performance of the underground cavern and thermal analyses are investigated [22].

Air, as a free and non-toxic working fluid, is a great choice for this mean. Air with a composition of 75.57% nitrogen, 23.16% oxygen, and 1.27%, has a critical temperature of about -140 ℃ while the temperature of LNG at atmospheric pressure is about -160 ℃. Such temperature difference is enough to liquefy air in the cryogenic condenser of a liquefied air power cycle. The technology of such power systems is similar to those used in the LAES systems [23].

Various studies investigated the coupling of renewable energies with CAES systems. Energy and exergy analyses of an ocean-based CAES system were presented by Patil and Ro [24]. The energy and exergy efficiencies were found to be 50 and 55%, respectively [24]. A novel integrated wind-solar based CAES system was investigated by Ji et al. [25]. The round trip and exergy efficiencies of the proposed system were 61.2% and 65.4%, respectively [25]. Mohammadi and Mehrpooya [26] investigated the coupling of a solar dish with the CAES system. The system consumed 152 kW during charging mode for compression of the air and by using the solar heat to increase the temperature of the gas turbine inlet, produced 228 kW during discharging mode [26]. Yang et al. [27] proposed an integration of a solar CAES system with combined heating, cooling, and power system for a hotel building in south China. The integrated system considered in their study included solar collector assembly, gas turbine cycle, absorption chiller, heat recovery steam generator unit, and CAES system. Solar collectors were utilized to increase the temperature of the air before entering the gas turbine unit to improve cycle efficiency. It was concluded that their proposed system enhanced the efficiency of previous systems by 1.01% [27]. Mahmoud et al. [28] reviewed the integration of various types of mechanical energy storage systems including flywheel, CAES, and pumped-hydro with solar and wind energy. They concluded that CAES systems due to their rapid startup time, low cost, stability, and flexibility are a good choice for integration with wind or solar energy [28].

In this study, a novel integrated CAES system including a solar power tower system using high temperature $(LiNaK)_2CO_3$ carbonate molten salt, combined power cycle, liquefied air power cycle, thermoelectric generator (TEG), and an LNG regasification unit is proposed. While the utilization of high-temperature molten salt to aid the CAES system has not been studied before but that was never joint with a liquefied air power cycle to improve the overall performance of the integrated system. Through energy and exergy analysis the performance of the proposed system evaluated. Also, a parametric study is carried out to investigate the effects of varying major design parameters on system performance. The results presented in this paper enable types, locations, and magnitudes of losses to be determined to reduce sources of inefficiency in energy conversion systems.

2. Methodology

As mentioned earlier, energy and exergy approaches are used for the thermodynamic analysis in this study [30]. MATLAB software integrated with REFPROP 9 library is utilized to develop a thermodynamic model used for the integrated system. The conservations of mass and energy for the steady-state condition are presented respectively as follows:

$$\sum \dot{m}_i - \sum \dot{m}_e = 0 \quad (1)$$

$$\dot{Q} - \dot{W} = \sum (\dot{m}h)_e - \sum (\dot{m}h)_i \quad (2)$$

Exergy rate balance at steady-state is expressed by:

$$\dot{E}x_W - \dot{E}x_Q = \sum (\dot{m}ex_f)_i - \sum (\dot{m}ex_f)_e - \dot{E}x_D \quad (3)$$

where $\dot{E}x_W$ and $\dot{E}x_Q$ are rates of exergy transfer accompanying heat transfer and work, respectively, and ex_f is the total flow exergy:

$$\dot{E}x_Q = (1 - \frac{T_0}{T_i})\dot{Q}_i \quad (4)$$

$$\dot{E}x_W = \dot{W} \quad (5)$$

$$ex_f = ex_{PH} + ex_{CH} + ex_{KE} + ex_{PT} \quad (6)$$

where ex_{PH}, ex_{CH}, ex_{KE}, and ex_{PT} denote physical, chemical, kinetic, and potential exergies.

3. Proposed System Description

Schematic of the diabatic solar-assisted CAES system is presented in Fig. 1. The integrated system comprises an air compression unit, thermal oil loop, solar power tower with thermal energy storage, gas turbine with a combustor, thermoelectric generator, liquefied air power cycle, and LNG regasification unit.

During charging mode, the air is pressurized by a double-stage air compressor to store the energy. Thermal oil leaving the cold tank is used in the intercooler and aftercooler units to recover the heat produced during the compression process. The recovered heat is then used during the discharging mode to increase the cycle performance. Compressed air is stored in the salt cavern at near ambient temperature. The heated thermal oil is stored in the hot tank. During discharging mode, the air flowing out of the cavern is firstly heated up in heater 1 by the thermal oil, and then in heater 2 by the high-temperature molten salt before entering the first stage of the gas turbine unit to generate power. High-temperature molten salt is a eutectic mixture of Li_2CO_3(32.1%)-Na_2CO_3(33.4%)-K_2CO_3(34.5%) and used as the heat transfer fluid in the solar power tower system and also for thermal energy storage [29]. After the first expansion process, the air enters the combustion chamber unit where natural gas is used to increase the temperature of the air before the next expansion process. For the base case, exhaust gases with a temperature of 1100 ℃ enter the second stage of the gas turbine unit to produce power. Exhaust gases of the second stage pass through the heater 3 to provide the required heat of the liquefied air power cycle. As the temperature of the flue gas leaving the heater 3 is still high, a thermo-electric generator is utilized to recover the remaining waste heat of the flue gas before discharging it to the environment at 150 ℃.

In the liquefied air power cycle, air is pressurized by the pump and enters two sequential heat exchangers where it is superheated before entering the turbine to generate power. The expanded air exits the turbine at a lower temperature (455 ℃ for the base case) and enters the recuperator where rejects heat to the pressurized cold air. The air at the exit of the recuperator, state 37 is a very low temperature of -109.6 ℃. At the same time, LNG exiting the tank is pressurized by the LNG pump for the regasification process. The temperature of the liquefied air power cycle condenser is a function of LNG temperature at the outlet of the pump. For the LNG regasification process, the natural gas must be heated up before entering the expander to increase the power yield of the regasification process. Therefore, LNG then goes through heater 4 to be heated up by the thermal oil. It then enters heater 5 which produces cooling before entering the natural gas expander. The natural gas leaves the system to be transported by pipeline.

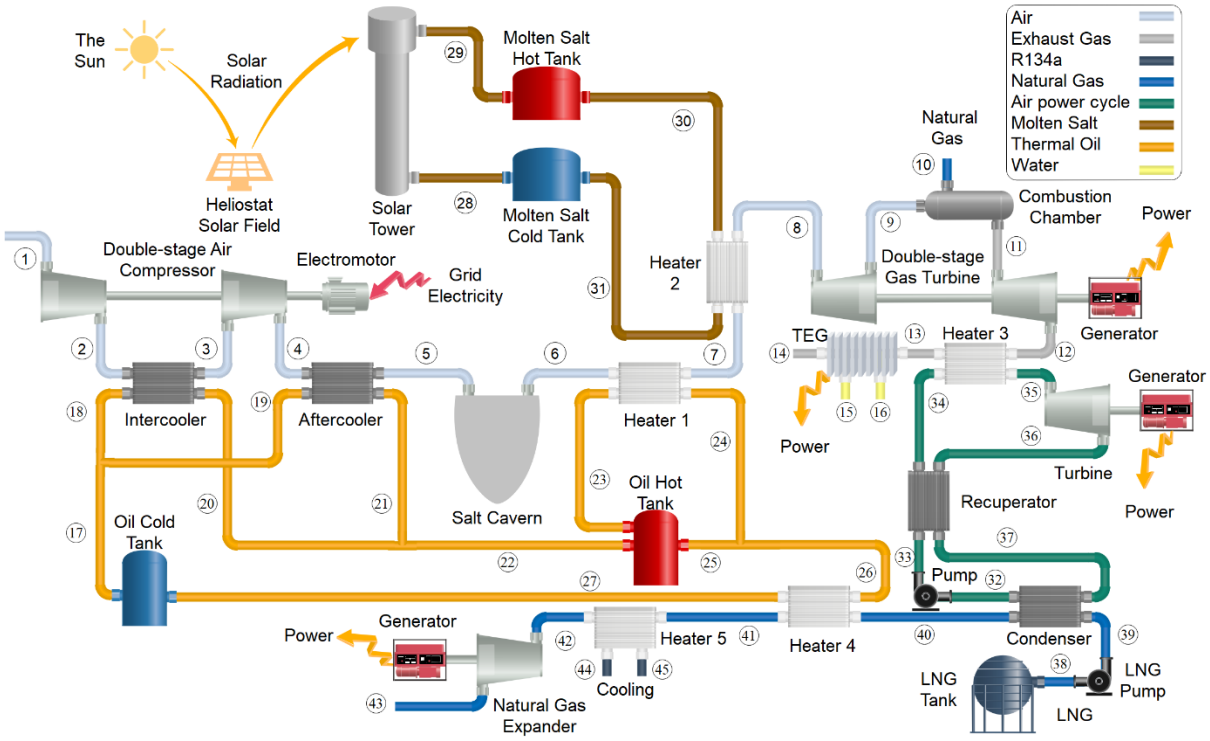

Figure 1 Schematic of the solar-assisted CAES system.

Input parameters for the base case of this study are presented in Table 1 [23, 30-33].

Table 1 Input parameters for the base case of this study.

Parameter	**Value**
Mass flow rate of air entering the system (kg/s)	100
Pressure ratio of each compression/expansion stage	6
Pinch point (℃)	10
Area of a single mirror (m^2)	100
Number of mirrors	400
Maximum solar irradiance (W/m^2)	976

Optical efficiency (%)	75
Wind velocity (m/s)	5
Molten salt type	$(LiNaK)_2CO_3$
Inlet temperature of molten salt (℃)	400
Outlet temperature of molten salt (℃)	700
Outlet temperature of combustor (℃)	1100
TEG figure of merit	0.8
Liquefied air power cycle turbine inlet pressure (kPa)	15000
Pressure of LNG tank (kPa)	130
Pressure of LNG pump outlet (kPa)	10000
Temperature of liquefied air power cycle condenser (℃)	$T_{39} + \text{pinch point}$
NG turbine outlet pressure (kPa)	7000
Isentropic efficiency of air compressors (%)	0.8
Isentropic efficiency of gas turbines (%)	0.86
Isentropic efficiency of liquefied air power cycle and NG turbines (%)	0.8
Isentropic efficiency of liquefied air power cycle and LNG pumps (%)	0.75

4. Analysis

Apart from the common mass, energy, and exergy balance equations a series of other equations are solved to complete the thermodynamic modeling of this study. The emitted heat from the sun is evaluated as follows [31]:

$$\dot{Q}_s = A \times n \times I \tag{7}$$

Here, A, n, and I represent the aperture area, number of mirrors, and irradiance, respectively. A portion of the heat from the sun is reflected by the mirrors while the remaining heat is wasted due to the optical efficiency of the mirrors [31]:

$$\dot{Q}_h = \dot{Q}_s . \eta_h \tag{8}$$

where η_h is the optical efficiency of the heliostat mirrors.

The rate of absorbed heat by the high-temperature molten salt is evaluated by calculating the heat losses associated with the receiver tower:

$$\dot{Q}_a = \dot{Q}_h - \dot{Q}_{l,total} = \dot{Q}_h - \dot{Q}_{l,cond} - \dot{Q}_{l,conv} - \dot{Q}_{l,e} - \dot{Q}_{l,r} \tag{9}$$

where $\dot{Q}_{l,total}$, $\dot{Q}_{l,cond}$, $\dot{Q}_{l,conv}$, $\dot{Q}_{l,e}$, and $\dot{Q}_{l,r}$ denote total heat loss of the receiver, conduction heat loss, convection heat loss, emission heat loss, and radiation heat loss, respectively.

Considering charging and discharging modes, each system component is studied using the first and second laws of thermodynamics.

The reaction that takes place in the combustion chamber is given by [17]:

$$\bar{\lambda}C_{x_1}H_{y_1} + \left(x_{N_2}N_2 + x_{O_2}O_2 + x_{Ar}Ar\right) \rightarrow y_{CO_2}CO_2 + y_{N_2}N_2 + y_{O_2}O_2 + y_{H_2O}H_2O + y_{Ar}Ar \quad (10)$$

Energy balance on the combustion chamber is expressed as follows:

$$\dot{n}_{Air}\bar{h}_{Air} + \dot{n}_{Fuel}LHV_{Fuel}M_{Fuel} = \dot{n}_{Product}\bar{h}_{Product} + (1-\eta_{CC})LHV_{Fuel}M_{Fuel} \quad (11)$$

where LHV_{Fuel} represents a lower heating value of the fuel.

The power consumed during charging, and also, the power produced during discharging mode are evaluated as follows:

$$\dot{W}_{charge} = \dot{W}_{AC,1} + \dot{W}_{AC,2} \quad (12)$$

$$\dot{W}_{discharge} = \dot{W}_{GT,1} + \dot{W}_{GT,2} + \dot{W}_{TEG} + \dot{W}_{LAPC,t} + \dot{W}_{NG,t} - \dot{W}_{LAPC,p} - \dot{W}_{LNG,p} \quad (13)$$

where subscript AC, GT, TEG, NG, LAPC, t, and p denote air compressor, gas turbine, thermoelectric generator, natural gas, liquefied air power cycle, turbine, and pump, respectively.

Cooling load produced during discharge is given as follows:

$$Q_C = \dot{m}_{45}(h_{45} - h_{44}) \quad (14)$$

Energy and exergy efficiencies of the integrated system are presented as follows:

$$\eta_I = \frac{\dot{W}_{discharge} + Q_C}{\dot{W}_{charge} + \dot{m}_{38}(h_{43} - h_{38}) + \dot{Q}_s + \dot{m}_{10}LHV} \quad (15)$$

$$\eta_{II} = 1 - \frac{\dot{E}x_{d,total}}{\dot{W}_{charge} + \dot{m}_{38}\left(ex_{f,38} - ex_{f,43}\right) + \dot{E}x_s + \dot{m}_{10}ex_{f,10}} \quad (16)$$

Normalized carbon dioxide emission is determined by:

$$\varepsilon = \frac{\dot{m}_{CO_2}}{\dot{W}_{net}} \quad (17)$$

Here, $\dot{m}_{CO_2}$ is the mass flow rate of carbon dioxide which is determined from the following equation:

$$\dot{m}_{CO_2} = \frac{\bar{\lambda} \times \dot{m}_9 \times M_{CO_2}}{M_{air}} \quad (18)$$

where M_{CO_2} and M_{air} denote the molar mass of carbon dioxide and air, respectively. Also, $\bar{\lambda}$ is the ratio of fuel to air on a molar basis [17]:

$$\bar{\lambda} = \frac{n_{Fuel}}{n_{Air}} \tag{19}$$

Energy and exergy balance equations for each component present in the proposed energy storage system are presented in Table 2.

Table 2 Energy and exergy balance equations for each component of the integrated system

Component	Energy balance equation	Exergy balance equation
Air compressor I	$\dot{W}_{AC,1} = \dot{m}_2 h_2 - \dot{m}_1 h_1$	$\dot{E}x_{D,AC,1} = \dot{m}_1 ex_1 - \dot{m}_2 ex_2 + \dot{W}_{AC,1}$
Air compressor II	$\dot{W}_{AC,2} = \dot{m}_4 h_4 - \dot{m}_3 h_3$	$\dot{E}x_{D,AC,2} = \dot{m}_3 ex_3 - \dot{m}_4 ex_4 + \dot{W}_{AC,2}$
Intercooler	$\dot{m}_2 h_2 + \dot{m}_{18} h_{18} = \dot{m}_3 h_3 + \dot{m}_{20} h_{20}$	$\dot{E}x_{D,IC} = \dot{m}_2 ex_2 + \dot{m}_{18} ex_{18} - \dot{m}_3 ex_3 - \dot{m}_{20} ex_{20}$
Aftercooler	$\dot{m}_4 h_4 + \dot{m}_{19} h_{19} = \dot{m}_5 h_5 + \dot{m}_{21} h_{21}$	$\dot{E}x_{D,AC} = \dot{m}_4 ex_4 + \dot{m}_{19} ex_{19} - \dot{m}_5 ex_5 - \dot{m}_{21} ex_{21}$
Heater I	$\dot{m}_6 h_6 + \dot{m}_{23} h_{23} = \dot{m}_7 h_7 + \dot{m}_{24} h_{24}$	$\dot{E}x_{D,H,1} = \dot{m}_6 ex_6 + \dot{m}_{23} ex_{23} - \dot{m}_7 ex_7 - \dot{m}_{24} ex_{24}$
Heater II	$\dot{m}_7 h_7 + \dot{m}_{30} h_{30} = \dot{m}_8 h_8 + \dot{m}_{31} h_{31}$	$\dot{E}x_{D,H,2} = \dot{m}_7 ex_7 + \dot{m}_{30} ex_{30} - \dot{m}_8 ex_8 - \dot{m}_{31} ex_{31}$
Gas turbine I	$\dot{W}_{GT,1} = \dot{m}_8 h_8 - \dot{m}_9 h_9$	$\dot{E}x_{D,GT,1} = \dot{m}_8 ex_8 - \dot{m}_9 ex_9 - \dot{W}_{GT,1}$
Gas turbine II	$\dot{W}_{GT,2} = \dot{m}_{11} h_{11} - \dot{m}_{12} h_{12}$	$\dot{E}x_{D,GT,2} = \dot{m}_1 ex_1 - \dot{m}_2 ex_2 - \dot{W}_{GT,2}$
Combustion chamber	$\dot{m}_9 h_9 + \dot{m}_{10} LHV_{Fuel} = \dot{m}_{11} h_{11} + (1 - \eta_{CC}) LHV_{Fuel}$	$\dot{E}x_{D,CC} = \dot{m}_9 ex_9 + \dot{m}_{10} ex_{10} - \dot{m}_{11} ex_{11}$
Heater III	$\dot{m}_{12} h_{12} + \dot{m}_{34} h_{34} = \dot{m}_{13} h_{13} + \dot{m}_{35} h_{35}$	$\dot{E}x_{D,H,3} = \dot{m}_{12} ex_{12} + \dot{m}_{34} ex_{34} - \dot{m}_{13} ex_{13} - \dot{m}_{35} ex_{35}$
LAPC turbine	$\dot{W}_{LAPC,t} = \dot{m}_{35} h_{35} - \dot{m}_{36} h_{36}$	$\dot{E}x_{D,LAPC,t} = \dot{m}_{35} ex_{35} - \dot{m}_{36} ex_{36} - \dot{W}_{LAPC,t}$
Recuperator	$\dot{m}_{33} h_{33} + \dot{m}_{36} h_{36} = \dot{m}_{34} h_{34} + \dot{m}_{37} h_{37}$	$\dot{E}x_{D,REC} = \dot{m}_{33} ex_{33} + \dot{m}_{36} ex_{36} - \dot{m}_{34} ex_{34} - \dot{m}_{37} ex_{37}$
Condenser	$\dot{m}_{37} h_{37} + \dot{m}_{39} h_{39} = \dot{m}_{32} h_{32} + \dot{m}_{40} h_{40}$	$\dot{E}x_{D,C} = \dot{m}_{37} ex_{37} + \dot{m}_{39} ex_{39} - \dot{m}_{32} ex_{32} - \dot{m}_{40} ex_{40}$
LAPC pump	$\dot{W}_{LAPC,p} = \dot{m}_{33} h_{33} - \dot{m}_{32} h_{32}$	$\dot{E}x_{D,LAPC,p} = \dot{m}_{32} ex_{32} - \dot{m}_{33} ex_{33} + \dot{W}_{LAPC,p}$
LNG pump	$\dot{W}_{LNG,p} = \dot{m}_{39} h_{39} - \dot{m}_{38} h_{38}$	$\dot{E}x_{D,LNG,p} = \dot{m}_{38} ex_{38} - \dot{m}_{39} ex_{39} + \dot{W}_{LNG,p}$
Heater IV	$\dot{m}_{26} h_{26} + \dot{m}_{40} h_{40} = \dot{m}_{27} h_{27} + \dot{m}_{41} h_{41}$	$\dot{E}x_{D,H,4} = \dot{m}_{26} ex_{26} + \dot{m}_{40} ex_{40} - \dot{m}_{27} ex_{27} - \dot{m}_{41} ex_{41}$
Heater V	$\dot{m}_{41} h_{41} + \dot{m}_{44} h_{44} = \dot{m}_{42} h_{42} + \dot{m}_{45} h_{45}$	$\dot{E}x_{D,H,5} = \dot{m}_{41} ex_{41} + \dot{m}_{44} ex_{44} - \dot{m}_{42} ex_{42} - \dot{m}_{45} ex_{45}$
Natural gas turbine	$\dot{W}_{NG,t} = \dot{m}_{42} h_{42} - \dot{m}_{43} h_{43}$	$\dot{E}x_{D,NG,t} = \dot{m}_{42} ex_{42} - \dot{m}_{43} ex_{43} - \dot{W}_{NG,t}$
Heliostat mirrors	$\dot{Q}_s = \dot{Q}_h + \dot{Q}_{l,opt}$	$\dot{E}x_{D,HM} = \dot{E}x_s - \dot{E}x_h$
Solar tower	$\dot{Q}_h = \dot{Q}_a + \dot{Q}_{l,cond} + \dot{Q}_{l,conv} + \dot{Q}_{l,e} + \dot{Q}_{l,r}$	$\dot{E}x_{D,ST} = \dot{E}x_h + \dot{m}_{28} ex_{28} - \dot{m}_{29} ex_{29}$
TEG	$\dot{W}_{TEG} = \dot{m}_{13} h_{13} + \dot{m}_{15} h_{15} - \dot{m}_{14} h_{14} - \dot{m}_{16} h_{16}$	$\dot{E}x_{D,TEG} = \dot{m}_{13} ex_{13} + \dot{m}_{15} ex_{15} - \dot{m}_{14} ex_{14} - \dot{m}_{16} ex_{16} - \dot{W}_{TEG}$

5. Results and Discussion

The results of the energy and exergy analyses of the integrated system proposed in this study are presented in Table 3. Using Eqs. 15 and 16, the energy and exergy efficiencies are found as 55.3% and 46.4%, respectively. Additionally, it is observed that for producing 99.7 MW of electricity during discharge at full load, 2.2 kg/s of fuel is required. The charging power required

for the compressors is 44.5 MW. The terms of Eqs. 12 and 13 are calculated by using the energy balance equations listed in Table 2. By applying the balance equations on the two air compressor, power required for the charging mode of plant is calculated. Also, the cooling load produced during discharging mode is calculated by Eq. 14. Moreover, by using the exergy balance equations listed in Table 2, the overall exergy destruction rate of the plant is found as 129.4 MW. In the next section of results and discussion, detailed results of the exergy analysis will be presented.

After determining the unknown species coefficients of the combustion process (see Eq. 10) and the molar based fuel to air ratio (see Eq. 19), the mass of produced carbon dioxide is calculated using Eq. 18. Finally, by knowing the net power generation of the plant, the normalized carbon dioxide emissions are calculated as 210.1 kg CO_2/MWh (see Eq. 17). Thermodynamic properties including temperature, pressure, enthalpy, and entropy for the various streams of the system are presented in Table 4. As mentioned earlier, for evaluating the thermophysical properties, REFPROP 9 library is utilized in this study. Also, energy balance equations listed in Table 2 are used to find unknown properties such as mass flow rate, enthalpy, temperature, or pressure. For instance, the enthalpy and temperature of state 8, are calculated from the energy balance equation for heater 2.

Table 3 The results of the thermodynamic analysis of the developed model in this study.

Parameter	**Value**
Energy efficiency (%)	55.3
Exergy efficiency (%)	46.4
Power consumption during charging (MW)	44.5
Power generation during discharging (MW)	99.7
Cooling power produced during discharging (MW)	52.9
Overall exergy destruction rate (MW)	129.4
Consumed fuel (kg)	2.2
Normalized carbon dioxide emissions (kg CO_2/MWh)	210.1

Table 4 Thermodynamic properties of various streams in the proposed solar-assisted CAES system.

Stream number	**Fluid**	**State of matter**	**Pressure (kPa)**	**Temperature (℃)**	**Enthalpy (kJ/kg)**	**Entropy (kJ/kg.K)**
1	Air	Gas	101.3	25.2	298.4	6.9
2	Air	Gas	506.5	240.3	517	6.9
3	Air	Gas	506.5	35.2	307.7	6.4
4	Air	Gas	2532.5	257.6	534.3	6.5
5	Air	Gas	2532.5	35.2	303.4	6
6	Air	Gas	2532.5	35.2	303.4	6
7	Air	Gas	2532.5	227	502.4	6.5
8	Air	Gas	2532.5	448.4	737.4	6.8
9	Air	Gas	506.5	227.8	504	6.9
10	Methane	Gas	101.3	25.2	910	6.7
11	Flue gas	Gas	506.5	1100	1484.1	8
12	Flue gas	Gas	101.3	714.6	1032.6	8.1
13	Flue gas	Gas	101.3	368.3	651.1	7.6
14	Flue gas	Gas	101.3	150	424.7	7.2

15	Water	Liquid	101.3	25.2	104.9	0.4
16	Water	Liquid	101.3	30.2	125.8	0.4
17	Therminol 66	Liquid	101.3	25.2	52.8	0.2
18	Therminol 66	Liquid	101.3	25.2	52.8	0.2
19	Therminol 66	Liquid	101.3	25.2	52.8	0.2
20	Therminol 66	Liquid	101.3	228.3	479.5	1.3
21	Therminol 66	Liquid	101.3	245.6	515.8	1.3
22	Therminol 66	Liquid	101.3	237	497.8	1.3
23	Therminol 66	Liquid	101.3	237	497.8	1.3
24	Therminol 66	Liquid	101.3	47.2	99	0.3
25	Therminol 66	Liquid	101.3	237	497.8	1.3
26	Therminol 66	Liquid	101.3	141.3	296.7	0.9
27	Therminol 66	Liquid	101.3	26.2	54.9	0.2
28	Carbonate salt	Liquid	101.3	400	644	1.5
29	Carbonate salt	Liquid	101.3	700	1127	2
30	Carbonate salt	Liquid	101.3	700	1127	2
31	Carbonate salt	Liquid	101.3	400	644	1.5
32	Air	Liquid	3401	-143.2	-0.6	4.1
33	Air	Gas	15000	-119.6	30.7	4.2
34	Air	Gas	15000	356.3	639.6	6.2
35	Air	Gas	15000	704.6	1030.2	6.7
36	Air	Gas	3401	455.5	745.4	6.8
37	Air	Gas	3401	-109.6	136.5	5.1
38	Natural gas	Liquid	130	-158.2	10.9	0.1
39	Natural gas	Gas	10000	-153.2	42.4	0.2
40	Natural gas	Gas	10000	-121.6	153.7	1
41	Natural gas	Gas	10000	-75	348.3	2.1
42	Natural gas	Gas	10000	15.2	778.8	3.9
43	Natural gas	Gas	7000	-7.9	745.5	4
44	R134a	Gas	101.3	25.2	424.5	1.9
45	R134a	Liquid	101.3	-60	123.2	0.7

The power consumption/generation of various components in the integrated system is shown in Fig. 2. The first and second stages of the air compressor unit consume 21.9 and 22.7 MW of electricity, respectively. The power produced by the first and second stages of the gas turbine are 23.3 and 46.1 MW, respectively. The difference is due to the inlet temperatures. Inlet temperatures of the first and second stages are 448.4 and 1,100 ℃, respectively. The turbine of the liquefied air power cycle also produces 28.41 MW of electricity which is quite significant, mainly due to the high heat addition and low heat rejection temperatures of this cycle. The power generated by the TEG for the waste heat recovery process is calculated as 6.6 MW. Moreover, the electric power consumed by the LNG and liquefied air power cycle pumps are 3.9 MW and 3.1 MW, respectively.

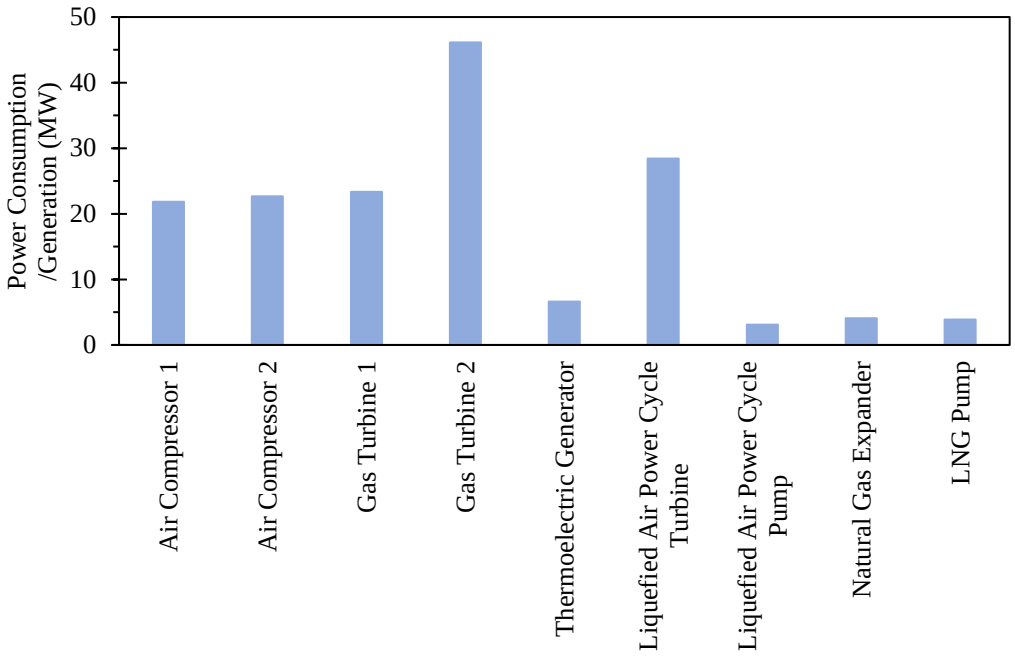

Figure 2 Power consumption/generation of various components in the integrated system.

Grid power storage and power generation of the energy storage system proposed in this study are shown in Fig. 3. From about 2 to 9 A.M., the demand profile of the selected location, which is the Bandar Abbas city located in southern Iran, is below the hourly average power demand. Therefore, the charging time of the plant for the grid power storage is set as 8 hours from 2 to 9 A.M. on full load. The power demand exceeds the average hourly demand from around 12 P.M., and reaches its peak at 3 P.M. Afterward, the demand reduces till 8 P.M., and increases again to reach its next local peak at 10 P.M. Therefore, the discharging phase of the CAES plant is set from 12 to 7 P.M. and from 9 to 11 P.M. The plant operates four hours on its half-maximum load and five hours at its maximum load.

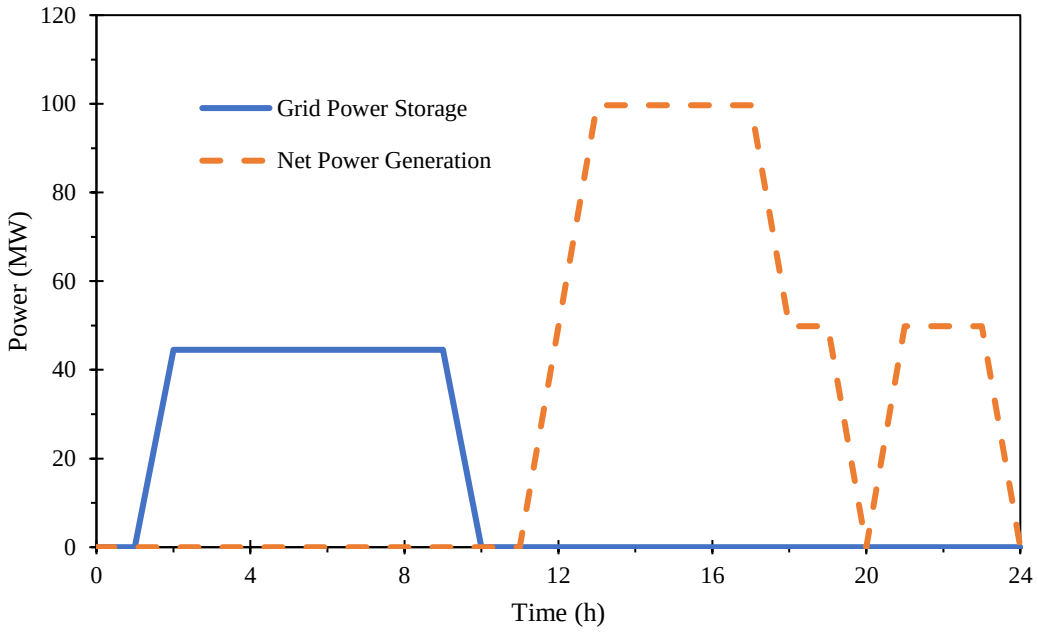

Figure 3 Grid power storage and power generation of the plant.

Exergy destruction rates of various components in the integrated system are presented in Fig. 4. As can be seen, the highest contributors to the overall exergy destruction rate of the system are the combustion chamber, heater 4, solar tower, recuperator, and heliostats with a value of 46.3, 20.6, 11.2, 10.2, and 8.7 MW, respectively. The high exergy destruction rate in the combustion chamber unit is due to the significant loss of available chemical exergy of the fuel during the combustion process. The significant exergy destruction rate of heater 4 is because of the high-temperature difference between the hot and cold streams of thermal oil and natural gas flowing through this heat exchanger. The exergy destruction of the solar tower unit is higher compared to heliostats because of the utilization of high-temperature salt. If a lower temperature salt is utilized, the exergy destruction of the solar tower unit will reduce.

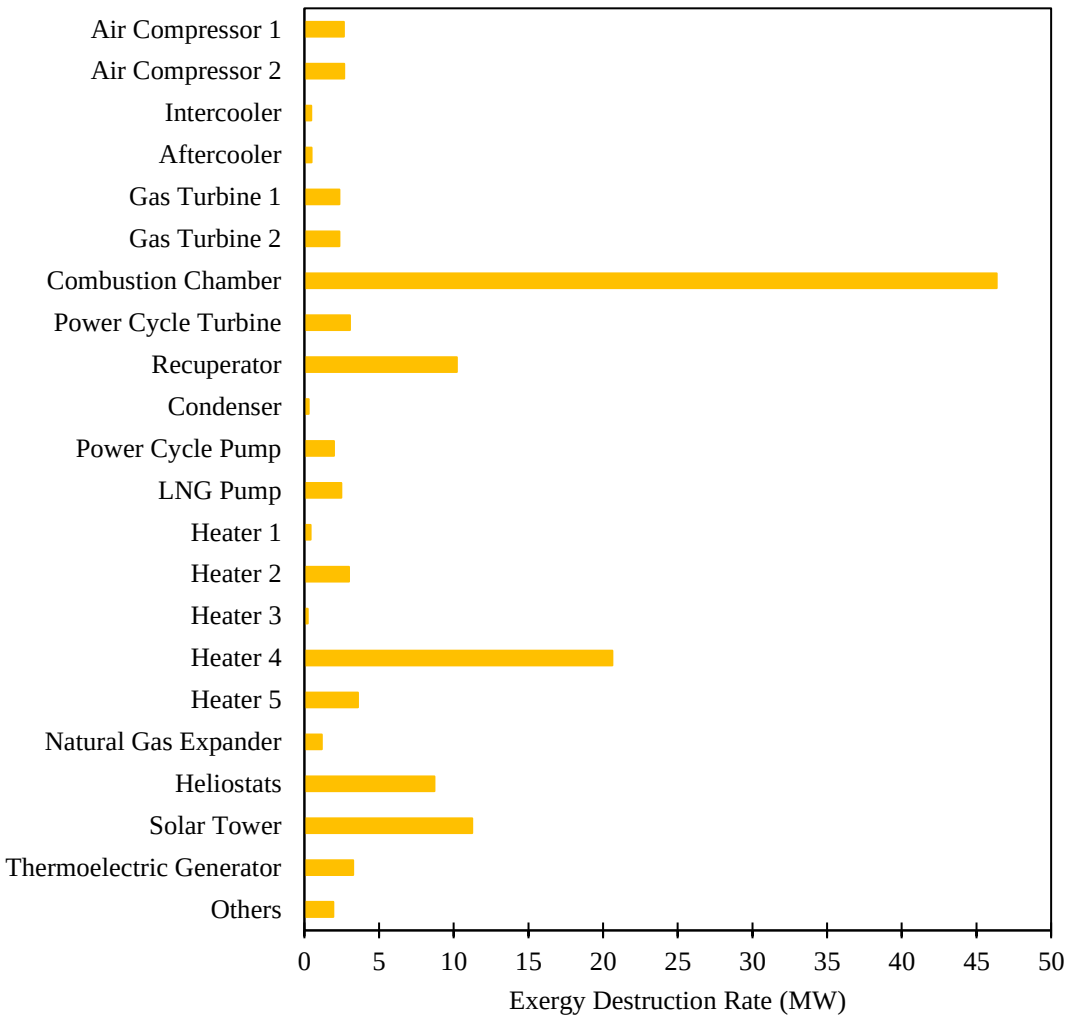

Figure 4 Exergy destruction rates of various components in the integrated system.

The effects of the gas turbines/compressors pressure ratios on the system performance are presented in Fig. 5. By increasing the pressure ratio of each stage of the compression/expansion process from 3 to 8, the energy efficiency reduces from 56.5% to 53.6%, while the exergy destruction rate increases from 126.6 to 136.8 MW. As the pressure ratio increases, more heat is stored by the thermal oil and hence, the exergy destruction in heater 1 is increased. However, due to the higher temperature of the air at state 7, the exergy destruction of heater 2 reduces. On the other hand, the outlet temperature of the air at state 9 reduces as the pressure ratio increases. It will result in more fuel consumption to achieve the fixed gas turbine inlet temperature at state 11. An increase in fuel consumption causes an aggravation of the exergy destruction rate of the integrated system.

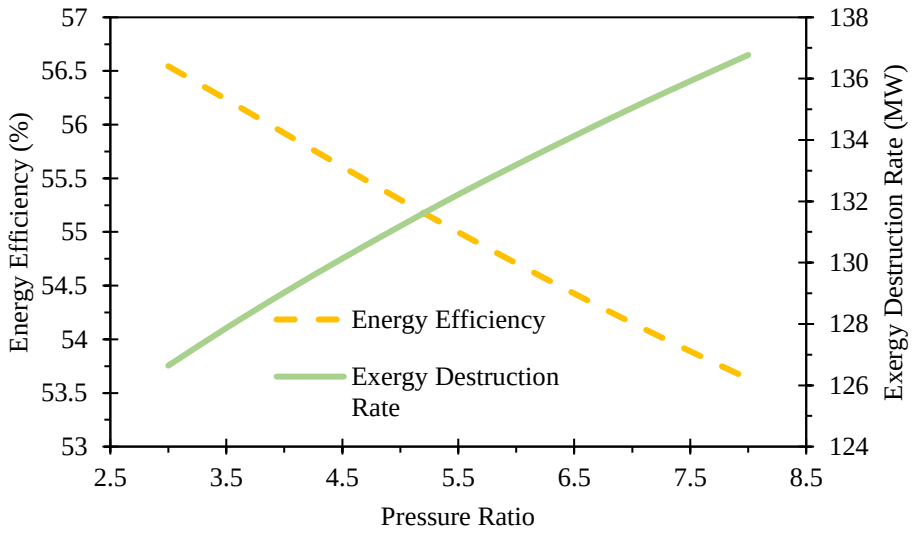

Figure 5 Effects of pressure ratio of each compression/expansion stage on the system performance.

The influences of increasing the heliostat numbers on fuel consumption and power generation of the system are presented in Fig. 6. When the heliostat numbers are increased from 300 to 850, the generated power increases from 99.8 to 109.5 MW, while the fuel consumption rate is reduced from 2.3 to 1.7 kg/s, respectively. This is because when the number of heliostats increases, the temperature of the air leaving heater 2 is increased drastically (from 391 to 695), and hence, the outlet temperature of the first stage gas turbine and its generated power are increased. Therefore, the fuel consumption rate in the combustion chamber is decreased.

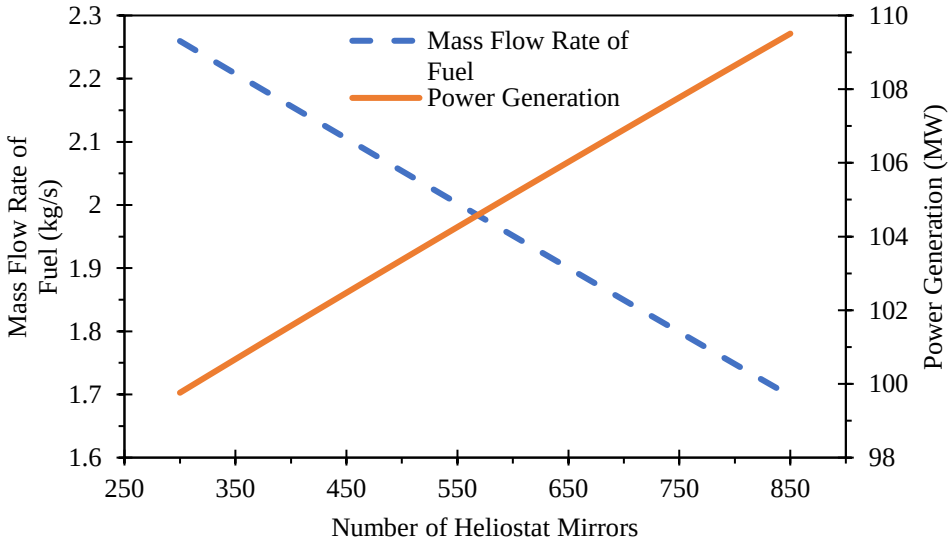

Figure 6 Influence of heliostat numbers on the integrated system performance.

The influence of the combustor outlet temperature on the system performance is presented in Fig. 7. When the combustion chamber outlet temperature increases from 1,000 to 1,400, the power

generated by the integrated system increases from 93.5 to 127.1 MW, and energy efficiency increases from 55.1% to 55.6%. As the combustor outlet temperature increases, the power output of the GT cycle increases. This causes an increase in the outlet temperature of the gas turbine which in turn results in an increase in power generation of the liquefied air power cycle and TEG unit. To be more specific, with the same amount of increase in the GTIT, the power generated by the TEG, liquefied air power cycle, and GT cycle are increased from 4.5, 22.9, and 65.9 MW to 14, 32.5, and 80.3 MW, respectively.

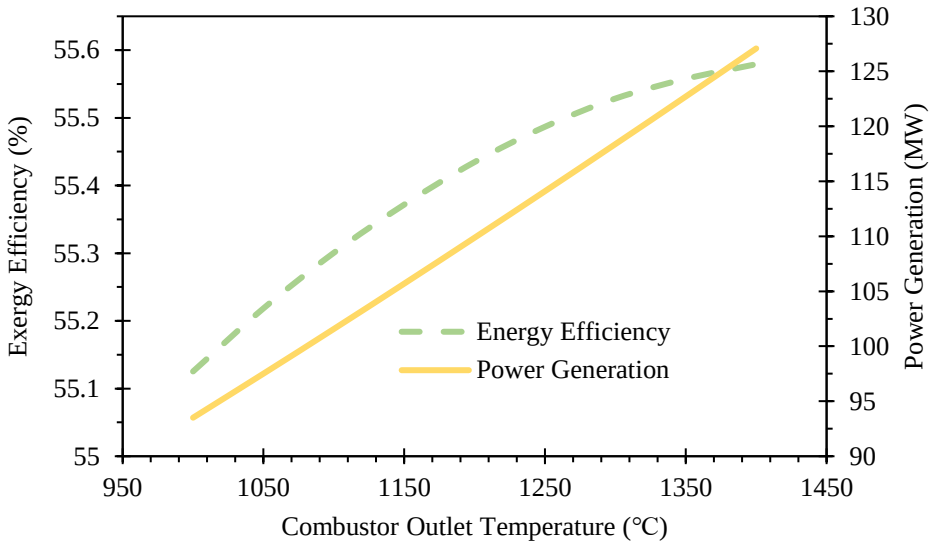

Figure 7 Influence of combustor outlet temperature on integrated system performance.

The influences of liquefied air power cycle turbine inlet pressure on the exergy destruction rate and generated power of the integrated system are shown in Fig. 8. As the inlet pressure of the liquefied air power cycle turbine increases from 5,000 to 18,000, the generated power increases from 92 to 102.6 MW, while the exergy destruction of the system is reduced from 168.5 to 127 MW, respectively. As the turbine inlet pressure increases, more heat is required in the liquefied air power cycle, and therefore, the temperature of flue gas leaving heater 3 is decreased. This translates into a more efficient consumption of the exergy content of the flue gas before discharging it to the atmosphere.

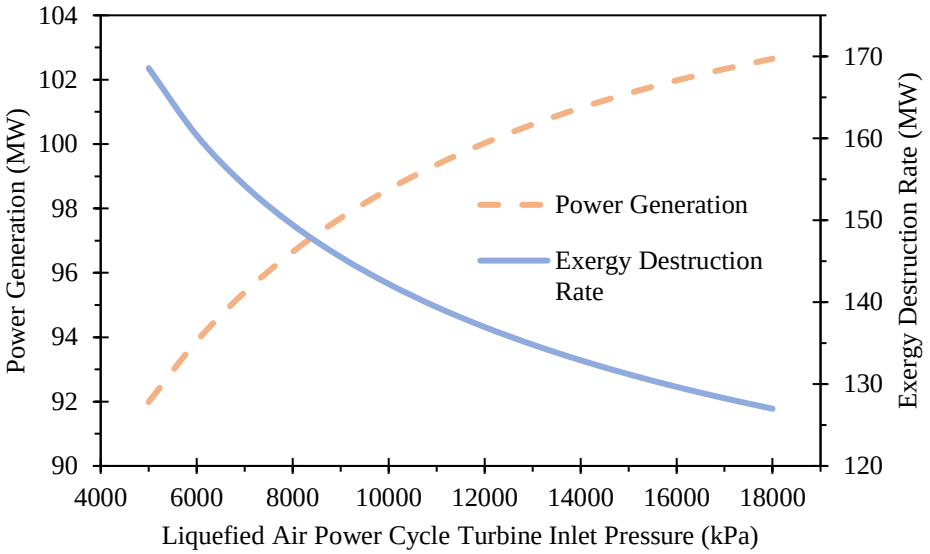

Figure 8 Influence of liquefied air power cycle turbine inlet pressure on integrated system performance.

The effects of LNG pump outlet pressure on the power generation and normalized CO_2 emissions of the cycle are presented in Fig. 9. The system is optimized at the LNG pump outlet pressure of 12,000 kPa. The optimum results of power generation and normalized CO_2 emissions are 102 MW and 209 kg CO_2/MWh, respectively. The liquefied air power cycle condenser temperature is dependent on the temperature of natural gas at the outlet of the LNG pump. The best performance of the liquefied air power cycle, and hence the integrated system is achieved at the LNG pump outlet pressure of 12000 kPa.

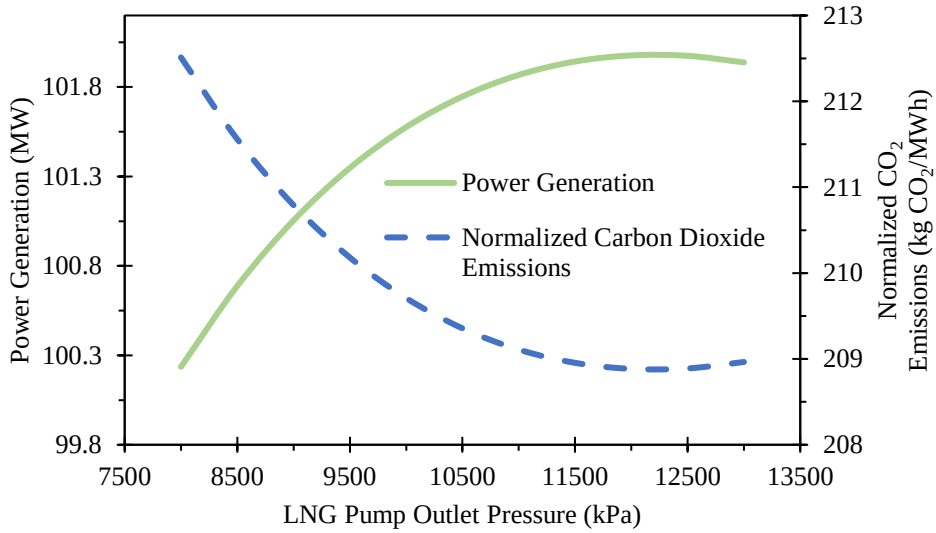

Figure 9 Effects of LNG pump outlet pressure on the integrated system performance.

6. Comparison with past studies

The energy and exergy efficiencies of the proposed solar-assisted CAES system are compared with those presented previously in Table 5. Past studies selected for comparison include a trigeneration CAES plant with absorption chiller and parabolic trough collectors [34], an advanced CAES system integrated with organic Rankine cycle/Kalina cycle for the waste heat recovery purposes [35], and a hybrid CAES system which uses both wind and solar energies [36]. It is shown that the integrated system proposed in this study has a better performance in terms of energy and exergy.

Table 5 A comparison between the present CAES system and past studies.

Study	Energy efficiency (%)	Exergy Efficiency (%)
Present study	54.9	46.9
Wang et al. [34]	53.1	45.4
Soltani et al. [35]	50.7-51.2	44.2-44.6
Chen et al. [36]	46.5	-

7. Conclusions

A novel solar-assisted diabatic compressed air energy storage system integrated with a liquefied air power cycle and a liquefied natural gas regasification system is designed and analyzed in this paper. The system comprises an air compression unit, thermal oil loop, gas turbine, solar power tower with thermal energy storage, liquefied natural gas regasification unit, thermoelectric generator, and liquefied air power cycle. The performance of the energy storage system is investigated using energy and exergy analyses. A parametric study is carried out to examine the effects of varying major design parameters on the overall system performance. Major findings are presented as follows:

- The energy and exergy efficiencies of the integrated system are 55.3% and 46.4%, respectively.
- 44.5 MW of power is consumed during charging mode and 99.7 MW of power is generated during the discharging mode. This indicates that the energy storage system proposed here uses less than half of the power it produces during the discharging mode with the aid of solar energy and cold waste heat of liquefied natural gas.
- Excess air is used in the combustion process to reduce fuel consumption and improve the performance of the energy storage system. It is observed that 2.2 kg/s of fuel is required during the discharging mode of the system.
- The normalized carbon dioxide emissions of the system are 210.1 kg CO_2/MWh. The current system is three times less harmful to the environment compared to the carbon impact of Iranian national grid.
- The highest contributors to the overall exergy destruction rate of the system are the combustion chamber, heater 4, solar tower, recuperator, and heliostats. Therefore, to improve environmental sustainability, these components require further investigation in future research.

- Increasing the pressure ratio of the compressors will reduce the performance of the plant, while increasing the combustion chamber outlet temperature will improve it. Also, the normalized carbon dioxide emissions of the plant are minimized at LNG pump outlet pressure of 12 MPa. Increasing the number of heliostat mirrors from 300 to 850 will increase the power generation of the plant 99.8 to 109.5 MW.

References

[1] Turkson, C., Acquaye, A., Liu, W., Papadopoulos, T. Sustainability assessment of energy production: A critical review of methods, measures, and issues. Journal of Environmental Management, 264, 110464, 2020.

[2] Suberu, M. Y., Mustafa, M. W., Bashir, N. Energy storage systems for renewable energy power sector integration and mitigation of intermittency. Renewable and Sustainable Energy Reviews, 35, 499-514, 2014.

[3] Palmer, G., Floyd, J. Energy Storage and Civilization: A Systems Approach (Vol. 40). Springer Nature, 2020.

[4] Akinyele, D. O., Rayudu, R. K. Review of energy storage technologies for sustainable power networks. Sustainable Energy Technologies and Assessments, 8, 74-91, 2014.

[5] Alami, A. H., Aokal, K., Abed, J., Alhemyari, M. Low pressure, modular compressed air energy storage (CAES) system for wind energy storage applications. Renewable Energy, 106, 201-211, 2017.

[6] Koohi-Fayegh, S., Rosen, M. A. A review of energy storage types, applications and recent developments. Journal of Energy Storage, 27, 101047, 2020.

[7] Budt, M., Wolf, D., Span, R., Yan, J. A review on compressed air energy storage: Basic principles, past milestones and recent developments. Applied Energy, 170, 250-268, 2016.

[8] Rufer, A. Energy storage: systems and components. CRC Press, 2017.

[9] Liu, H., He, Q., Saeed, S. B. Thermodynamic analysis of a compressed air energy storage system through advanced exergetic analysis. Journal of Renewable and Sustainable Energy, 8(3), 034101, 2016.

[10] Krawczyk, P., Szabłowski, Ł., Karellas, S., Kakaras, E., Badyda, K. Comparative thermodynamic analysis of compressed air and liquid air energy storage systems. Energy, 142, 46-54, 2018.

[11] Peng, H., Yang, Y., Li, R., Ling, X. Thermodynamic analysis of an improved adiabatic compressed air energy storage system. Applied Energy, 183, 1361-1373, 2016.

[12] Liu, J. L., Wang, J. H. A comparative research of two adiabatic compressed air energy storage systems. Energy Conversion and Management, 108, 566-578, 2016.

[13] Zhao, P., Wang, J., Dai, Y. Thermodynamic analysis of an integrated energy system based on compressed air energy storage (CAES) system and Kalina cycle. Energy Conversion and Management, 98, 161-172, 2015.

[14] Szablowski, L., Krawczyk, P., Badyda, K., Karellas, S., Kakaras, E., Bujalski, W. Energy and exergy analysis of adiabatic compressed air energy storage system. Energy, 138, 12-18, 2017.

[15] Carriveau, R., Ebrahimi, M., Ting, D. S. K., McGillis, A. Transient thermodynamic modeling of an underwater compressed air energy storage plant: Conventional versus advanced exergy analysis. Sustainable Energy Technologies and Assessments, 31, 146-154, 2019.

[16] Sadreddini, A., Fani, M., Aghdam, M. A., Mohammadi, A. Exergy analysis and optimization of a CCHP system composed of compressed air energy storage system and ORC cycle. Energy conversion and management, 157, 111-122, 2018.
[17] Moran, M. J., Bailey, M. B., Boettner, D. D., Shapiro, H. N. Fundamentals of engineering thermodynamics. 9th Edition, Wiley, 2018.
[18] Ghorbani, B., Miansari, M., Zendehboudi, S., Hamedi, M. H. Exergetic and economic evaluation of carbon dioxide liquefaction process in a hybridized system of water desalination, power generation, and liquefied natural gas regasification. Energy Conversion and Management, 205, 112374, 2020.
[19] Xue, F., Chen, Y., Ju, Y. A review of cryogenic power generation cycles with liquefied natural gas cold energy utilization. Frontiers in Energy, 10(3), 363-374, 2016.
[20] Zhang, Y., Yao, E., Zhang, X., & Yang, K. Thermodynamic analysis of a novel compressed carbon dioxide energy storage system with low-temperature thermal storage. International Journal of Energy Research. 44, 6531‐6554, 2020
[21] Saputro, E. A., Farid, M. M. Performance of a small-scale compressed air storage (CAS). International Journal of Energy Research, 43(12), 6233-6242, 2019
[22] Karapekmez, A., Dincer, I., Javani, N. Development of a new integrated energy system with compressed air and heat storage options. Journal of Energy Storage, 32, 101955, 2020
[23] Lee, I., Park, J., Moon, I. Conceptual design and exergy analysis of combined cryogenic energy storage and LNG regasification processes: Cold and power integration. Energy, 140, 106-115, 2017.
[24] Patil, V. C., Ro, P. I. Energy and exergy analysis of ocean compressed air energy storage concepts. Journal of Engineering, 2018.
[25] Ji, W., Zhou, Y., Sun, Y., Zhang, W., An, B., Wang, J. Thermodynamic analysis of a novel hybrid wind-solar-compressed air energy storage system. Energy Conversion and Management, 142, 176-187, 2017.
[26] Mohammadi, A., Mehrpooya, M. Exergy analysis and optimization of an integrated micro gas turbine, compressed air energy storage and solar dish collector process. Journal of Cleaner Production, 139, 372-383, 2016.
[27] Yang, C., Wang, X., Huang, M., Ding, S., Ma, X. Design and simulation of gas turbine-based CCHP combined with solar and compressed air energy storage in a hotel building. Energy and Buildings, 153, 412-420, 2017.
[28] Mahmoud, M., Ramadan, M., Olabi, A. G., Pullen, K., Naher, S. A review of mechanical energy storage systems combined with wind and solar applications. Energy Conversion and Management, 210, 112670, 2020.
[29] Vignarooban, K., Xu, X., Arvay, A., Hsu, K., Kannan, A. M. Heat transfer fluids for concentrating solar power systems–a review. Applied Energy, 146, 383-396, 2015.
[30] Borgnakke, C., Sonntag, R. E. Fundamentals of Thermodynamics. 10th Edition, Wiley, 2019.
[31] Xu, C., Wang, Z., Li, X., Sun, F. Energy and exergy analysis of solar power tower plants. Applied Thermal Engineering, 31(17-18), 3904-3913, 2011.
[32] An, X., Cheng, J., Zhang, P., Tang, Z., Wang, J. Determination and evaluation of the thermophysical properties of an alkali carbonate eutectic molten salt. Faraday discussions, 190, 327-338, 2016.

[33] Wang, X., Yang, C., Huang, M., Ma, X. Multi-objective optimization of a gas turbine-based CCHP combined with solar and compressed air energy storage system. Energy Conversion and Management, 164, 93-101, 2018.
[34] Soltani, M., Nabat, M. H., Razmi, A. R., Dusseault, M. B., Nathwani, J. A comparative study between ORC and Kalina based waste heat recovery cycles applied to a green compressed air energy storage (CAES) system. Energy Conversion and Management, 222, 113203, 2020.
[35] Chen, J., Liu, W., Jiang, D., Zhang, J., Ren, S., Li, L., Li, X., Shi, X. Preliminary investigation on the feasibility of a clean CAES system coupled with wind and solar energy in China. Energy, 127, 462-478, 2017.
[36]Tavanir Organization. Electrical industry. 2015. Available online at: https://amar.tavanir.org.ir/pages/report/stat95/index.html. [Accessed 19 December 2020]